# Estimates of Condensed Water in and Energetics of the Hunga Volcanic Plume on 15 January 2022

McNutt, S.R.[1], E.R. Williams[2], F.J. Spera[3], and M.A. Scruggs[4]

[1]School of Geosciences, University of South Florida, Tampa, Florida, USA

[2]MIT Department of Civil and Environmental Engineering, Cambridge, Massachusetts, USA

[3]Department of Earth Science and Earth Research Institute, University of California Santa Barbara, Santa Barbara, California, USA

[4]Geology Department, Wichita State University, Wichita, Kansas, USA

Corresponding Author: S.R. McNutt, smcnutt@usf.edu

## Abstract

Systematic calculations are made for the volume of the January 15, 2022 Hunga plume. We use inferred atmospheric water concentrations to estimate the mass of $H_2O$ condensate in the plume. A cylinder 58 km high (early) and radius 15 km for the core and a disk 10 km thick for the umbrella cloud provide an estimate of the plume volume. 1.3-5 g/m$^3$ as the water concentration for the core and 1.3 g/m$^3$ for the umbrella cloud give the $H_2O$ plume loading. The 58-km-high (maximum) plume height was transient, and the huge umbrella cloud reached a maximum 30-60 min later. Although the thickness of the umbrella cloud is poorly known, it is likely thicker near the volcano and thinner at leading edges. Plume volume estimates were made every 10 minutes, coinciding with the timing of satellite images, and the peak values were recorded when the umbrella reached its maximum size at 0520 UTC. Umbrella thicknesses were assumed to be 10 km. Lidar images (Calipso) show thickness of the ash-rich part of the plume to be 2-2.5 km. The estimates for the mass of water range from 2.7 to 3.5 x $10^{12}$ kg. Estimates for magma volume range from 1.8 to 5 km$^3$. An upper estimate of the amount of water in pristine andesitic magma, using 2600 kg/m$^3$ density, 3-5 wt % water, and 6.85 km$^3$ magma, is 5.4-8.9 x $10^{11}$ kg, a factor of 3-4 lower than the plume water content. We thus infer that circa 80 percent of the water in the plume is from seawater flashed to steam.

These estimates constrain the source characteristics, seeking agreement in mass and heat using an isentropic explosive energy model. These include magma eruptive volume, plume water content, magma reservoir initial conditions, the heat needed to flash seawater to steam, and the explosive yield. The observed and modelled explosion energy of the 2022 Hunga eruption is comparable to that of Krakatau in 1883 (~100-200 Mt TNT), despite Hunga eruption being 2 to 4 times less voluminous. This contrast is explained by the ingestion of copious amounts of seawater and its subsequent vaporization and expansion compared to the drier Krakatau eruption.

## Introduction

The eruption of Hunga Volcano on 15 January 2022 was one of the largest volcanic eruptions worldwide in the past 140 years, and marks the first time since Krakatau in 1883 that an eruption produced Lamb waves and associated meteotsunamis that encircled the globe (Henley et al, 2024; Matoza et al., 2022). The eruption produced the highest known ash column at 58 km (Van

Eaton et al., 2023; Mastin et al., 2024, K. Bedka, writ. comm.), and a huge umbrella cloud that was ≥500 km in diameter (Smart, 2022; Le Mével et al., 2023; Mastin et al., 2024). The eruption was complex in that the primary vent at the initiation of the main phase of the eruption was at 150 m depth below sea level (Yuen et al., 2022). Copious amounts of water were conspicuously involved in the eruption (Millan et al., 2022; Võmel et al., 2022; Zhu et al., 2022; Mastin et al., 2024; Wu et al., 2025) and this, coupled with the submarine eruptive vent, has led to the view that phreatomagmatism is the underlying mechanism. An alternative hypothesis to phreatomagmatism has been proposed by Henley et al (2024) who argue for the build-up of magmatic fluids at depth over a protracted timeframe due to crystallization and concomitant volatile exsolution and degassing of prior magma batches and sealing of the system by mineral precipitation before catastrophic failure by hydraulic fracture. Although the details of the mechanism by which seawater encountered the magma body leading to explosive eruption warrants further investigation, phreatomagmatism as envisaged by Wohletz (1986) remains a viable mechanism and is our working hypothesis.

Figure 1 shows a map of the locations of Hunga Volcano and its surroundings. Hunga Tonga and Hunga Ha‘apai are the two islands still above sea level on 14 January 2022, the day before the climactic eruption, while Hunga Volcano is the name for the main edifice. Study of the eruption has been hampered by the fact that there were no geophysical instruments on the island itself, as the nearest calibrated instruments were located 757 km away in Fiji (Yuen et al., 2022). The lack of nearby stations was compensated for by the fact that many of the signals were strong and showed up clearly on distant stations. Continuous satellite data captured by GOES 17 and Himawari 8 (Carr et al., 2022; Horvath et al., 2024; Smart, 2022), and open-access data generated by networks of seismometers and infrasound instruments were readily available (Matoza et al., 2022; Yuen et al., 2022; Zheng et al., 2023). Many of the signals were strong and showed up clearly on distant stations. Data on lightning occurrence from the global VLF network GLD360 were available in summary form shortly after the eruption (Van Eaton et al., 2023; C. Vagasky, writ. comm.; R. Said, writ. comm.).


*Figure 1. Map of the study area. The largest island, home to the Kingdom's capital Nuku'alofa, is noted with a white arrow, and the white star shows the location of Hunga Volcano. Imagery Source: ArcGIS Online World Imagery Basemap, EarthStar Geographics.*

At the time of this writing (Fall 2025; nearly four years after the eruption) numerous preliminary studies have been published, answering many initial questions. A reasonable estimate of the volume of ejecta is 6.85 $km^3$, constrained by deposit volumes on the ocean floor and changes in bathymetry (Clare et al., 2023; Seabrook et al., 2023; Henley et al., 2024; Kelly et al., 2024; Wu et al., 2025). Multiple studies of infrasound, seismic, atmospheric, geomagnetic, and tidal data have been analyzed to provide constraints on the "size" of the eruption. The yield was estimated to be 61 Mt based on 'intense atmospheric pressure waves and scaling arguments' (Diaz and Rigby, 2022), although values ranging from 15 to 200 Mt have been published (Adushkin et al., 2022; Kulichkov et al., 2022; Vergoz et al., 2022; Donner et al., 2023; Purkis et al., 2023). Estimates of infrasound pressures were given by Matoza et al. (2022) and Yuen et al. (2022), and the magnitudes and mechanisms of the seismic events by Poli and Shapiro (2022), Yuen et al. (2022), Zheng et al. (2023), and Kitner et al., (2023). The amount of water *vapor* in the plume was quite significant, approximately 9% of the atmospheric global total at the time of the eruption, based upon satellite data (Millan et al., 2022; Zhu et al., 2022; Vomel et al., 2022; Xu et al., 2023). The visible water in satellite images (such as Figure 2) consisted of water droplets and inferred ice particles (Pavolonis et al., 2020; Mastin et al., 2024, p.64 and their figures 7 and 8).

In this paper we provide estimates of the amount of water in the plume in condensate form, which we then use to constrain the volume of magma needed to reproduce observed eruption parameters. We first show calculations of the amount of water in the plume using simple geometric constructs and straightforward assumptions. We then use these numbers along with estimates of the volume of erupted magma to determine the amount of magma-derived water versus seawater in the plume. We use phase-equilibria modeling, thermodynamic relations, and calorimetry to calculate how much magma was needed to flash the estimated amount of seawater to steam. Finally, we model the explosion yield using the inferred magma and water volumes and suitable assumptions for depth, pressures, proportions of $H_2O$ in the phreatomagma, and other eruption parameters. The term phreatomagma is defined here as a mixture of pristine magma, including its juvenile volatile content (i.e., magmatic volatiles) plus a fraction of volatiles (mainly $H_2O$) derived from an exogenous source such as groundwater or in this case seawater.

## Data and Methods

The main data used to estimate the amount of water were GOES 17 visible images that were taken every 10 minutes, complemented by Himawari 8 images (Carr et al., 2022; Horvath et al., 2024; Smart, 2022). These were used to make time-dependent estimates of plume water, although the maximum values were recorded late in the sequence. Strictly speaking, these images show the area of the top of the expanding umbrella cloud taken from above at a slightly oblique angle (Fig. 2.). The dark shadows of the eruption cloud on the Earth's surface and on the umbrella cloud are especially discernible later in the sequence. We measured umbrella cloud diameter at two perpendicular places (maximum and orthogonal) to the nearest km, then converted to obtain radii. Because the plume was approximately elliptical in shape, we used the formula $A = \pi ab$ to calculate cloud area. We note that the central portion of the plume above the vent was often much higher than the majority of the plume, but it represents only a small portion of the entire area. The core represented most of the volume at 0410 UTC, 13-22 percent from 0420-0420 UTC, but less than 3.3 percent from 0440 UTC onwards. By 0500 UTC the total plume volume had reached 84 percent of the final value, increasing to 91 percent at 0510 UTC and 100 percent at 0520 UTC (Appendix C).

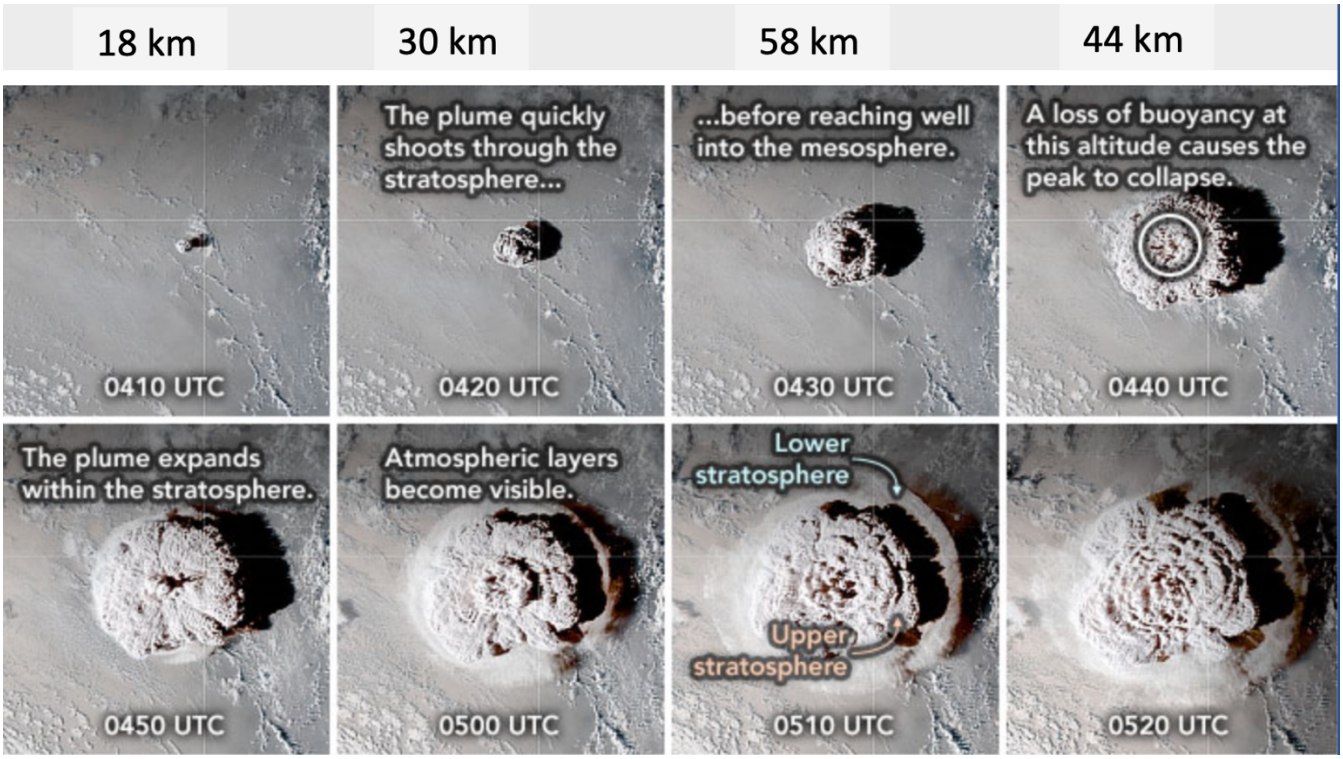


*Figure 2. GOES-17 images of the eruption every 10 minutes from 0410 to 0520 UTC. The irregular areas are the upper surface of the plume. A lower skirt cloud is partly visible in the last 4 images. The dark areas to the right are shadows from the Sun (off to the left). From Thompson et al. (2022). See Appendix C for horizontal dimensions.*

We estimate plume dimensions using the few images available showing the Hunga plume from the side (Mastin et al., 2024). For comparison, we examined lateral views of several Alaskan and other eruptions. An example of a lateral view of a plume from Redoubt Volcano is shown as Figure 3. The top of the main part of the plume is 12 km altitude, and it can be seen that the vertical dimension of the umbrella portion of the plume is 25-33% of the height. We used these values in our calculations (ex: a plume 40 km high was assumed to have an umbrella portion that was ~10 km thick). See Appendix A for further details.

*Figure 3. April 1990 eruption of Redoubt Volcano. Source: AVO image database. This is a mature plume, tens of minutes after the eruption onset and similar in relative time to the Hunga plume at 0520 UTC. Note the thickness of the umbrella portion is 25-33 percent of the height.*

**Plume Volume estimates**

Using measured heights, areas, and assumed thicknesses, a straightforward scheme was used to estimate plume volume. A plume geometry consisting of a core (the central tallest portion) and one or more disks (the umbrella portion), as depicted in Figure 4 was implemented. The core had a radius of 15 km, based on photographs of the Hunga plume from Mastin et al. (2024) and photographs of numerous other eruption plumes (AVO image database). The peak plume height was measured (same values as shown in Figure 2, top) on satellite images by Carr et al. (2022). The volume of the core is its area times its height and the volume of the disk is area * thickness, with area $A = \pi ab$ and the thickness = ¼ * height. We then summed the core volume and disk at each time step of 10 minutes to provide an estimate of total plume volume (see Appendix A).

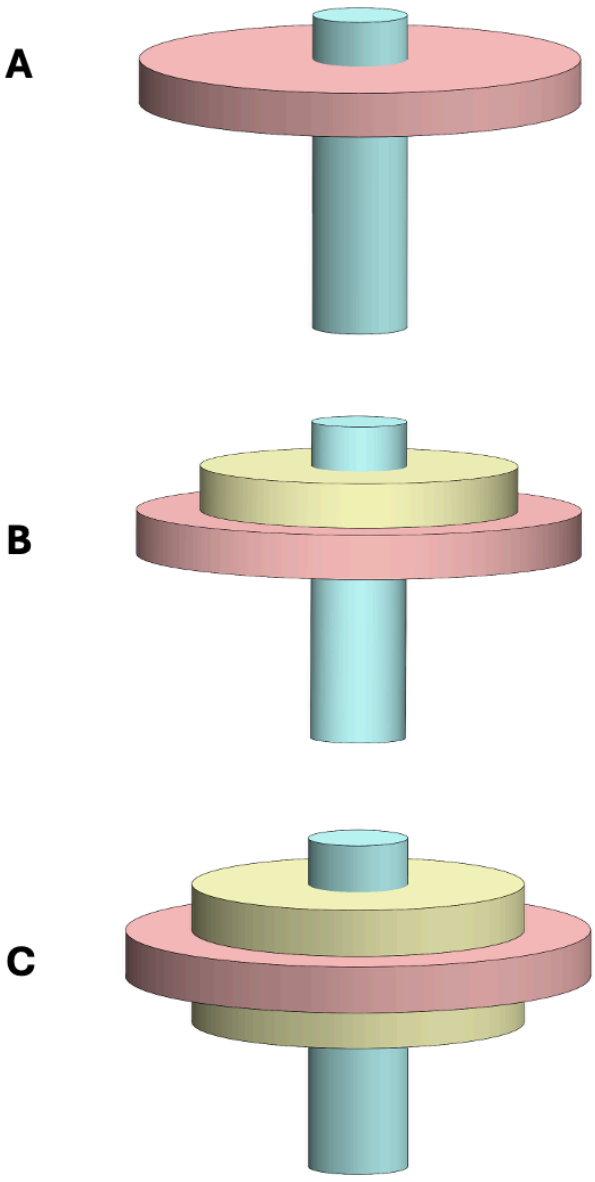


*Figure 4. Schematic diagrams of plume showing the core and umbrella cloud portions. We used these three geometries to be able to determine the effects of variations and uncertainties in the estimates. A-core + disk; B-core + 2 disks; C- core + 3 disks. The figure sequence does not represent evolution of the plume with time. The colors are only used to highlight the different parts of the plume.*

Although we assumed the thickness of the umbrella portion of the plume (1/4 x height), we can provide a few additional constraints on that parameter. Calipso data (Baron et al., 2023; Dogan et al., 2023) showed the ash-rich portion of the plume to be about 2-3 km thick at longitudes from 159 to 161.5 deg E (3000 to 2720 km from the vent; the ash was also detected over Reunion Island, 1000s of km W of the vent; these were several days after the eruption). We infer, based on the 2D images showing side views (Dogan et al., 2023) that the ash-rich portion is the central thinner part, and the total plume is thicker with the upper and lower parts dominated by water

and ice. Additionally, Gupta et al. (2022) showed schematic diagrams of a 2- and 3-part ash cloud (their Figure 4), and their thickness estimates are similar to our estimate of h/4. Their more realistic view of the plume is thicker near the vent and thins outwards. Our usage of a disk is a simpler geometry (hence easier to modify) and gives comparable volumes.

**Water Concentration**

Volume estimates of the plume are just one component of the problem addressed. To determine the total amount of water, we also need to estimate the concentration of water in both the disk and core.

For the core (higher concentrations) we consider the example of the subaerial eruption of Augustine (Appendix A) that determines observed plume geometries and known ash volumes and mass measurements. We measure the maximum height of the plume and the radius at several different heights, producing several cylinders that are then added together to estimate the total volume (see Appendix A). In the case of Augustine, the top of the volcano is 1.1 km above sea level, and the top of the main part of the plume was 10 km above sea level. The volume of ash that fell on the ground was estimated as $1.7 \times 10^6$ $m^3$ (Coombs et al., 2010; J. Power, pers. comm.). We assume that the ash contains 5 wt.% $H_2O$, a value consistent with melt inclusions in the andesite composition of the Augustine ash (Coombs et al., 2010), and near the maximum $H_2O$ contents recorded by plagioclase-hosted melt inclusions in Hunga tephra (Wu et al., 2025). Then we multiply the 5 wt.% $H_2O$ by the mass of erupted ash to estimate the mass of magmatic water in the plume. We divide the mass by the volume and normalize to g of water per $m^3$ of air.

The result of this calculation for Augustine volcano shows that the mean cloud water content (CWC) is about 0.7 $g/m^3$. This is within the range of typical values for thunderstorms (Williams and McNutt, 2005; see also below and Appendix B). These are values when the plume is near the vent and the time of observation is near the eruption onset. As time progresses, the plume becomes less water-rich as surrounding air is entrained. Hence, we use the mean value of the peak values for thunderstorms of 1.3 $g/m^3$ for the core in our calculations for Hunga, as well as a higher value of 5 $g/m^3$ for comparison. The 5 $g/m^3$ is an estimate; we know the water concentration is high right after the eruption onset, but we do not have a measured value. Although this value is twice the high value for a typical thunderstorm (see Appendix B), we note that an assumption of the above Augustine calculation is that "the ambient atmosphere is completely dry" (Williams & McNutt, 2005)–which is not likely the case at Hunga. The typical relative humidity of the boundary layer air over the tropical ocean is 80% (Shakespeare and Roderick, 2024). This corresponds to a water vapor concentration of 2.4 $g/m^3$ at 30 deg C.

For the umbrella cloud, we use estimates of water concentrations that are based on measurements of thunderclouds. These are of comparable size and we infer that the concentrations are representative. We compiled data on CWC for ordinary thunderstorms from five studies (Dye et al., 1986; Dye et al., 1988; Weinheimer et al., 1991; Stith et al., 2006; Heymsfield et al., 2009). The peak values for the various thunderstorms range from 0.3 to 2.5 $g/m^3$, with a mean of 1.3 $g/m^3$ and a median of 1.0 $g/m^3$. We used the mean value of 1.3 $g/m^3$ for our calculations (Appendix B). An earlier study by Geotis (1971) showed radar data for 8 thunderstorms, with a mean of 1.0 $g/m^3$, consistent with the value used here.

Note that these are identical to our lower estimates for the core, resulting in a single value of 1.3 $g/m^3$ in our estimates for water concentrations in the plume. This acknowledges that the plume becomes more dilute as it expands, but by an unknown amount. Hence, both the thicknesses and water concentrations are functions of distance away from the vent. However, we have chosen to use fixed thicknesses and concentrations for the modeling for computational simplicity. The effects of volume and concentration likely offset each other, so we have chosen simple geometries and uniform concentrations for computational ease and appropriateness where highly accurate water concentrations are unavailable.

Examples of calculations of the amount of water in the full plume (core and disk) are shown in Table 1 for 0520 UTC when the plume is fully developed. Our full set of calculations is presented in Appendix C for eight different time steps. The height of the core is taken from Carr et al., (2022; see also Figure 2). The radius of the core is held fixed at 15 km (Mastin et al., 2024). The two diameters are shown as measured from the satellite images, and the radii are assumed to be one half of these. The area is determined using the formula for an ellipse (as discussed in the previous section) which is a close approximation and likely within 1 percent. The thickness is held constant at 10 km for the full disk for the first model. A second model was also run, dividing the disk into two parts, each 5 km thick (Figure 4B), with different radii and different $H_2O$ concentrations. This is a simple scheme to evaluate how variations in the calculated and assumed values trade-off in the overall calculations. Note that the volume of the disk is two orders of magnitude greater than that of the core.

*Table 1. Calculations of volumes of the plume and total amount of water. See also Appendix C.*

| Time UTC | Part of plume | diam a, km | diam b, km | radius a, km | radius b, km | Ht km | Thick-ness km | Vol Km | gm $H_2O$ per $m^3$ | gm $H_2O$ in layer | Total $H_2O$ gm |
|---|---|---|---|---|---|---|---|---|---|---|---|
| 0520 | Umb-rella | 479 | 538 | 241 | 269 | 33 | 10 | $2x10^6$ | 1.3 | $2.64x10^{15}$ | |
| Fig 4A | core | | | 15 | 15 | 33 | 33 | $2.3x10^4$ | 1.3 | $3.03x10^{13}$ | $2.67x10^{15}$ |
| | | | | | | | | | | | |
| 0520 | Umb-rella 1 | 479 | 538 | 241 | 269 | 33 | 5 | $1x10^6$ | 1.3 | $1.32x10^{15}$ | |
| Fig 4B | Core | | | 15 | 15 | | 33 | $2.3x10^4$ | 5 | $1.17x10^{14}$ | |
| | Umb-rella 2 | 479 | 538 | 241 | 269 | | 5 | $1x10^6$ | 2 | $2.02x10^{15}$ | $3.46x10^{15}$ |

A second independent example calculation was made of the amount of magmatic water involved. Here we used the published values of 6-6.85 $km^3$ for the total volume of ejecta (Clare at al., 2023; Kelly et al., 2024; Henley et al., 2024; Wu et al., 2025). These were based on volume

estimates of the caldera as well as tephra and other materials deposited on the ocean floor. Assuming this entire volume is juvenile magma, we convert to mass using a density of 2600 kg/m$^3$, then multiply by 0.05 (assumes 5 wt.% $H_2O$; Plank et al., 2013; Brenna et al., 2022; Wu et al., 2025) to get the mass of magmatic water. Results of this calculation are shown in Table 2. These calculations estimate an upper limit for at least two reasons: it is likely a small volume is older rock and not juvenile magma (Seabrook et al., 2023), and plagioclase-hosted melt inclusions within the 2022 tephra estimate maximum pre-eruptive $H_2O$ contents at ~4.59 wt.% $H_2O$ (Wu et al., 2025). Alternatively, our volumes are estimated from the most active hour of an approximately 11-hour-long eruption (Van Eaton et al., 2023), and additional magma may have erupted after the main explosive phase considered herein.

*Table 2. Calculations of the amount of water contained in the magma. We start with volume, then multiply by assumed density to obtain mass, then multiply by the mass fraction of water (assumed).*

| Rock (km$^3$) | Density of magma (kg/m$^3$) | Mass (kg) | Water Mass fraction | Water Mass (g) | Mass water in 6 km$^3$ (g) | Mass water in 6.85 km$^3$ (g) |
|---|---|---|---|---|---|---|
| 1 | 2600 | $2.6x10^{12}$ | 0.03 | $7.8x10^{13}$ | $4.7x10^{14}$ | $5.4x10^{14}$ |
| 1 | 2600 | $2.6x10^{12}$ | 0.05 | $1.3x10^{14}$ | $7.8x10^{14}$ | $8.9x10^{14}$ |

Finally, we compare the amount of water from our plume estimates with the amount we calculate to be available from the erupted volume of magma. We find that the total amount of condensed water in the fully developed plume, $2.7x10^{12}$ kg (Table 1) is a factor of ~3 higher than the amount in the magma ($8.9x10^{11}$ kg). In other words, 67% of the water in the plume is seawater. If we use 3% rather than 5% for the wt. % of magmatic water ($5.4x10^{11}$ kg), then seawater accounts for 80% of the total plume. If we use the higher value of water of $3.5x10^{12}$ kg and the lower magmatic water estimate (3) then the percent sea water is 85%. Wu et al., (2025) reached a similar conclusion. Two papers provide additional evidence for seawater involvement. Colombier et al. (2025) demonstrated that $\delta^{34}S$ and $\delta^{37}Cl$ of ash particles erupted on 15 January 2022 cannot be explained without the involvement of large amounts of seawater. The same conclusion was reached by Wu et al. (2025) using measured S concentrations in olivine-hosted melt inclusions to constrain the amount of seawater required to reproduce the low observed $SO_2$ within the eruption plume. We interpret this as a further feature supporting of our model, indicating significant involvement of seawater. Our study agrees with these previous works on the importance of seawater in the Hunga eruption, and disagrees with the primarily magmatic-water model of Henley et al. (2024).

**Alternate calculations on condensed water**

We are aware of three recently published papers that constrain water vapor contents of the Hunga plume using data from NASA's Aura satellite. The satellite detects water vapor, a colorless, odorless gas that is detected by its spectral characteristics. These three studies show 146 $\pm$5 Tg of water vapor ($1.46x10^{14}$ g; Millan et al., 2022); >100 Tg of water vapor, (Zhu et al.,

2022); and >50 Tg of water vapor (Vomel et al., 2022). All three of these values are significantly smaller than our estimates, however, the water vapor should be added to the plume estimates to determine the total mass of water substance in the plume since our estimates apply to $H_2O$ in condensed form. Some water vapor likely came from evaporation and sublimation of rising condensate. Further, some water vapor may have cooled and condensed. Unfortunately, we have no measurements for either of these.

We emphasize again that water vapor is a colorless, odorless gas. What we address in our calculations is condensed water vapor in the form of liquid water droplets and ice particles in the plume under visible light (Pavolonis et al., 2020). In a sense, this is a comparison between different entities, as above, because some condensate is evaporated to produce some of the water vapor, and some water vapor is cooled to form condensate. Data to constrain this balance are needed for full elucidation.

We performed additional calculations (below and Table 3) based on insights from volcanic lightning. The numbers are for total water and are considerably higher than the estimates given above. Estimates of the amount of precipitation water per flash have been made by Petersen and Rutledge (1998). The implicit assumption here is that a volcanic eruption is a dirty thunderstorm and so is electrically powered by water substance (Cimarelli et al., 2022).

*Table 3. Estimates of the amount of water based on number of lightning flashes after Petersen and Rutledge (1998). Flash estimates come from Vaisala's GLD360 VLF network.*

| Region | Constant Kg/flash | g/flash | No. flashes | Total water, g |
|---|---|---|---|---|
| US | $1x10^8$ | $1x10^{11}$ | $4x10^5$ | $4x10^{16}$ |
| Tropical Pacific | $1x10^{10}$ | $1x10^{13}$ | $4x10^5$ | $4x10^{18}$ |
| Arid SW | $6x10^7$ | $6x10^{10}$ | $4x10^5$ | $2.3x10^{16}$ |

These estimates are higher (in other words more water in the plume), but they are based on cloud-to-ground (CG) lightning and rainfall (Petersen and Rutledge, 1998). Note that intra-cloud (IC) flash energy may be much less than for CG flashes (Rakov and Uman, 2003). The Hunga plume contained mostly suspended water and ice, and the massive rates of IC lightning were likely governed by gravity-wave initiated turbulence in the eruption plume (van Eaton et al., 2023). Thus, this comparison may not be warranted.

**Limitations**

There are significant sources of uncertainty in the estimates we have presented.
We believe the plume volume estimates are good to ±10%. We used simplified geometries (e.g. Fig. 4) for computational ease because exact values are not known. The main parameter is diameter, which we measured to the nearest km (<1 % error). The thickness is estimated based on comparison with published photographs of plumes from other volcanoes.

The biggest unknown is the cloud water content (CWC). We introduced a novel method applying CWC for thunderstorms to volcanoes. There are no direct measurements, so we used published values from thunderstorms, which are measured in the troposphere. However, much of the Hunga volcano disk cloud is stratospheric. We have assumed the same concentration but with a likely phase change (ice instead of liquid water). The Augustine volcano value (0.7 $g/m^3$) is in the middle of thunderstorm values, and it is also tropospheric.

The concentration within the plume likely has a gradient, higher near the core and lower with distance, but we assumed a constant value for ease of computation. We suggest that the gradient and size offset each other (the estimated concentration is too low near the core, and the volume is too high near the edges of the plume).

The erupted magma volume is estimated from the literature and is likely accurate to ±10%. The estimates of magma water content come from two sources; melt inclusions (3 wt. %) and assumed values from prior studies (5 wt. %; references above). Regardless, the conclusion that circa 80 % of the $H_2O$ in the plume came from sea water is robust.

A full formal error analysis does not appear to be warranted because too many quantities need to be estimated. We used what we consider to be the most likely values.

Additionally, more volcanic examples of CWC are needed, similar to the Augustine example in the Appendix. However, this topic is worthy of a separate larger effort.

## Discussion

Water concentration estimates provide constraints for modeling magma expansion and eruption. We first examine how much magmatic heat is needed to produce the amount of water in the plume. We follow this with models of the explosive yield.

### Eruption thermal calorimetry: internal energy and enthalpy requirements for sea water heating and vaporization.

How much heat is needed to vaporize seawater into steam? We know the temperature of the surface ocean water in Tonga in January (28 °C; Folland et al., 1997). The heat needed to raise the temperature of liquid water from 28 °C to 100 °C is thus 293 kJ/kg. To this is added the latent heat of vaporization of 2278 kJ/kg. The properties of $H_2O$ are taken from Haar et al., (1984). Multiplying the total mass of water determined earlier ($2.7 \times 10^{12}$ kg) times the latent plus sensible heats gives the total amount of thermal energy required to bring seawater to its boiling point and then vaporize it of $7.2 \times 10^{15}$ kJ. Now, magma has an effective isobaric specific heat that includes a sensible and latent component of 2000 J/kg K for Tonga magma using thermodynamic data in Lesher and Spera (2015). It starts out hot (estimated to be 1100 °C) and releases heat as it undercools and partially crystallizes to 100 °C. This estimate takes into account that some melt quenches to a glass and hence does not deliver its latent heat. The amount of magma needed to provide the necessary heat required for the water-steam generation by the magmatic heat yields a mass of magma of roughly $3.6 \times 10^{12}$ kg. This is an order of magnitude estimate only and does not consider details of the mechanisms involved. This mass, divided by

the magma density (dense rock equivalent (DRE) is assumed to be 2600 kg/m$^3$) yields volumes of magma of 1.4 km$^3$. These values agree with prior estimates based on bathymetry changes (most tephra was deposited as pyroclastic flows on the ocean floor; Clare et al., 2023, Kelly et al., 2024; Wu et al., 2025) and they also agree with independent estimates of the explosive yield outlined below. We think that significant heat exchange occurred between sea water and tephra that remained below sea level.

This simple formulation assumes 100 percent efficiency of converting magmatic heat to steam, which cannot be true in practice since energy is lost to heating air and magma fragmentation, among other effects (Wohletz, 1986; Henley et al., 2024). A value of 50-60 % efficiency may be more realistic (Maeno et al., 2022). In Table 4 we use ~50 % efficiency to determine the high-water estimate of 5.8 x 10$^{12}$ kg requiring 2.9 km$^3$ of magma. If the volume of magma is 5 km$^3$ (as modeled below), then this would imply that the efficiency was ~30 %. A magmatic temperature of 1100 °C was assumed, but the actual value may be higher or lower. We used the value of the effective specific heat for Hunga magma which includes a component to account for some microlite and nanolite (very small crystals in the groundmass) crystallization during eruption and quenching as well as some quench glass formation. Thermodynamic parameters were taken from Lesher and Spera (2015).

*Table 4. Values of parameters used for calorimetry calculations. Low and high refer to the lower and upper estimates for the total water in the plume (see preceding paragraph).*

| **Variable** | **low water estimate** | **high water estimate** |
|---|---|---|
| Water sensible enthalpy (28-100 C) | 293.2 J/kg | 293.2 J/kg |
| Water enthalpy of vaporization | 2278 kJ/kg | 2278 kJ/kg |
| Water mass | 2.7 x 10$^{12}$ kg | 5.8 x 10$^{12}$ kg |
| Water starting temperature | 28 °C | 28 °C |
| Steam temperature | 100 °C | 100 °C |
| Water enthalpy requirement | 7.2 x 10$^{18}$ J | 1.5x10$^{19}$ J |
| Magma effective specific heat | 2000 J/kg K | 2000 J/kg K |
| Magma initial temperature | 1100 °C | 1100 °C |
| Magma final temperature | 100 °C | 100 °C |
| Volume of magma needed | 1.4 km$^3$ | 2.9 km$^3$ |
| Yield based on internal energy | 1606 Mt | 3322 Mt |
| Yield based on enthalpy | 1720 Mt | 3561 Mt |

The amount of water in the magma is assumed to be 5 wt.% for arc andesitic magma (Plank et al, 2013; Sisson and Grove, 1993). This is a maximal value based on global average arc $H_2O$ contents (average 3.8 wt.% $H_2O$, Volcano A max 4.9 wt.% $H_2O$; Plank et al., 2013), plagioclase-melt hygrometry of pre-2022 Hunga Volcano eruptive products (4.6-5.1 ±0.4 wt.% $H_2O$; Brenna et al., 2022), experiments on comparable magmas at nearby Tongan volcanoes (2.3-5 wt.% $H_2O$; Brenna et al., 2022, and references therein), and tephra (0.7-3.0 wt.% $H_2O$ in metastable matrix glass; Wu et al., 2025) and phenocryst-hosted melt inclusions (0.6-4.6 wt.% $H_2O$; Wu et al., 2025) erupted on 15 January 2022. Still, as magma ascends to the surface some exsolved $H_2O$ may be lost from the melt by degassing. Water solubility in melt is a strongly decreasing function of pressure with a weak dependence on temperature. Although equilibrium during very rapid ascent may not be maintained perfectly, degassing is kinetically quite rapid. One realistic estimate of magmatic $H_2O$ might be ~2-3 wt. % (Brenna et al., 2022; Wu et al., 2025), however, pre-eruptive $H_2O$ estimates for magma supplying the 15 January 2022 eruption peak at 4.6 wt.% $H_2O$ (Wu et al., 2025). Thus, for our simple model, a rough approximation of 5 wt.% $H_2O$ in the pre-eruptive magma is reasonable. We chose a maximum limit for magmatic $H_2O$ so that our estimate of the seawater contribution will be a minimum; we also compare this result with a lower value (Table 2).

How good are size comparisons with Krakatoa, Katmai, Pinatubo, etc.? The gravity wave and atmospheric effects produced by the 15 January 2022 climactic eruption, coupled with similar estimates of explosive yield and devastating tsunami, make it directly comparable to the 1883 eruption of Krakatoa (Matoza et al., 2022; Yuen et al., 2022; Purkis et al., 2023; Mastin et al., 2024; Henley et al., 2024). The Hunga estimated volume of 6.85 $km^3$ is comparable, but note that the record-high plume for Hunga suggests this eruption was more explosive, with yields as high as 200 Mt (Adushkin et al., 2022; Diaz & Rigby, 2022; Kulichkov et al., 2022; Vergoz et al., 2022).

The Hunga plume rose very rapidly (100 to 350 m/sec; Mastin et al., 2024) and the estimated ash fall, determined from sampling on nearby islands, was only 0.1-0.2 $km^3$ (Mastin et al., 2024; Van Eaton et al., 2023). Volume changes in sea floor topography were large (up to 10 $km^3$; Seabrook et al., 2023). This suggests that the bulk of deposits remained on the ocean floor, and the heat transfer from magma to seawater occurred in the upper ~0.7 km of the ocean, just above the vent which apparently deepened during the eruption (0.15 to 0.85 km depth).

**Explosive Yields: a simple model**

As a consistency test on the plume/water content estimates, we consider a simple analytical model treating the eruption as a phreatomagmatic explosion (Wohletz, 1986; Zimanowski et al., 2015). We use the term ‘phreatomagma’ to refer explicitly to the multi-phase mixture of magma and supercritical volatiles at shallow depths during the eruption; this term is not used to imply the source of any involved water. The purpose is to compute explosion yield for a range of reasonable initial conditions including the particle to fluid mass ratio of the phreatomagma, the volume of magma treated as a two-phase mixture of particles + fluid, and the initial temperature and pressure of the magma. The term ‘particle’ here refers to all incondensable components of the plume including glass shards, melt droplets, cryptocrystalline tephra, crystals, and lithics.

This calculation assumes isentropic expansion (adiabatic and reversible) of the phreatomagma as it decompresses from a shallow reservoir to ambient or near-ambient pressure.

Yield estimates from the model can be compared with the energy estimates from tsunami and meteotsunami of ~20 Mt (Purkis et al., 2023; Chernogor & Luo, 2025), the energy of the atmospheric blast wave estimated 61-200 Mt (Adushkin et al., 2022; Diaz & Rigby, 2022; Kulichkov et al., 2022; Vergoz et al., 2022), and the thermal energy required to convert sea water to vapor, estimated here at ~2600 Mt. The latter value was computed by determining the enthalpy difference between liquid $H_2O$ at 298 K, heating it to 373 K and then vaporizing , all at 1 bar total pressure. The conversion from joules to Mt TNT used the standard conversion factor. The energy released by the surface-wave magnitude 5.8 seismic event is very small compared to the energy associated with ocean water motions (tsunamis) and deposited in the atmospheric by blast waves and thermal effects (see Figure 5 legend for details).

**Details of the modeling**

A fully coupled 2-or 3D model of the mechanics and thermodynamics of submarine phreatomagmatic eruptions is beyond the scope of this study. Several recent studies that address some of the pertinent issues may be found elsewhere (e.g., Cahalan and Dufek, 2021; Zheng et al., 2023; Schmid et al., 2022; Maeno et al., 2022). The explosive expansion of compressed phreatomagma can be treated as an isentropic process to a first approximation which is sufficient for the purposes of estimating the $H_2O$ content of the plume and comparing model explosion energy with aforementioned estimates.

A simple explosion model is sketched here. From the combined laws of thermodynamics, the specific internal energy of phreatomagma can be written in terms of the entropy and volume of the mixture in differential form as $de = Tds - pdv$ where e, s and v represent the specific internal energy, entropy and volume, respectively of phreatomagma, taken here as a mixture of particles (melt drops, glass shards, microcrystalline solids, crystals, lithic fragments) and a fluid phase ($H_2O$; see Zimanowski et al., 2015). Since the expansion is isentropic and the internal energy of the mixture depends on temperature only, $-\Delta e = \int_{v_o}^{v_{exit}} pdv = \int_{T_o}^{T_{exit}} \left(\frac{c_{Vf}+\delta c_c}{(1+\delta)}\right) dT$. The initial state is compressed phreatomagma at $p_o$, $T_o$ (volume $v_o$) and the final state is $p_{exit}=p_a$ and $T_{exit}$ where $p_a$ is either ambient atmospheric pressure for subsonic phreatomagma exit velocities or slightly larger for choked flows (10-50 bars; Buresti and Casarosa, 1989) or the hydrostatic pressure due to a column of water overlying the vent (initially at ~150 m below sea level and deepening syn-eruption) as in a submarine eruption. The line integral which is the negative of the internal energy change (the explosion energy) can be written in terms of the specific isochoric heat capacity, temperature $T_o$ and mass of the phreatomagma $M_o$ based on a particle-fluid 'dusty gas' model (Rudinger, 1976; Wallis, 1969) because the specific internal energy of the phreatomagma, a mixture of magma plus seawater, is independent of volume. This volume independence occurs because when $H_2O$ is treated as an ideal gas, an excellent approximation at magmatic temperatures and $p \lesssim 100$MPa, it has the well-known property $\left(\frac{\partial E}{\partial V}\right)_T = 0$ . Similarly, the condensed phase in the two-phase mixture of melt droplets, glass fragments and crystals, is essentially incompressible and therefore possess an internal energy

independent of pressure (or volume) at constant temperature. Hence the energy of the phreatomagmatic explosion can be written

$$-\Delta E = \frac{p_o V_o}{(1-\gamma)}\left[1-\left(\frac{p_a}{p_o}\right)^{\frac{(\gamma-1)}{\gamma}}\right] = \frac{c_{Vf}+\delta c_c}{(1+\delta)}\rho_o T_o V_o\left[1-\left(\frac{p_a}{p_o}\right)^{\frac{(\gamma-1)}{\gamma}}\right] \qquad (1).$$

Here, $V_o$ and $\rho_o$ represent the phreatomagma volume and initial density in the compressed (initial) state, $p_o$ and $T_o$ are the initial pressure and temperature and $p_a$ is the ambient pressure to which the mixture expands isentropically. The parameters $c_{Vf}$ , $c_{pf}$ and $c_c$ are the isochoric and isobaric specific heat capacities of fluid and the isobaric specific heat of particles (melt or solid, denoted by subscript 'c'), respectively , and $\delta = \frac{1-\phi_f}{\phi_f} = \frac{\phi_c}{1-\phi_c}$ where $\phi_f$ and $\phi_c$ are the mass fractions of fluid and particles in phreatomagma with heat capacity ratio $\gamma = \frac{c_{pf}+\delta c_c}{c_{Vf}+\delta c_c}$.

Examination of Eq (1) reveals that given the initial conditions, $p_o$, $V_o$, $\delta$, and the isochoric and isobaric specific heat of fluid and specific heat of particles, the explosion energy can be calculated. In this model, the initial density of phreatomagma is $\rho_o = \frac{\rho_f(1+\delta)}{1+(\rho_f/\rho_c)\delta}$ where the density of the fluid, $\rho_f$ (pure $H_2O$) is treated as an ideal gas, a good approximation in the p-T range of model applicability (Haar et al, 1984). Parameter values and definitions are given in Table 5; the range of the variable parameters are explicit on Figures 5 and 6. Once vent (exit) pressure ($p_v$) is specified, vent (exit) temperature ($T_v$) is determined using the relationship between temperature and pressure changes during the isentropic expansion, $T_v^{-1} p_v^{\left(\frac{\gamma-1}{\gamma}\right)} = T_o^{-1} p_o^{\left(\frac{\gamma-1}{\gamma}\right)} = \text{constant}$ using the appropriate value of the heat capacity ratio $\gamma$ for the phreatomagma.

*Table 5. Parameters for thermodynamic modelling.*

| PARAMETER | NAME | TYPICAL VALUE/UNITS |
|---|---|---|
| $c_{pf}$ | Isobaric specific heat of $H_2O$ at $T_o$ | 2540 J/kg K |
| $c_{Vf}$ | Isochoric specific heat of $H_2O$ at $T_o$ | 2071 J/kg K |
| $c_c$ | Specific heat capacity of particles | 1400 J/kg K |
| $T_o$ | Initial temperature of phreatomagma | 1300 K |
| $V_o$ | Initial volume of phreatomagma | variable $m^3$ |
| $M_o$ | Initial mass of phreatomagma | variable kg |

| | | |
|---|---|---|
| $\rho_o$ | Initial density of phreatomagma (= $M_o/V_o$) | variable kg/m$^3$ |
| $\rho_f$ | fluid density $\rho_f = \frac{p}{TR_f}$ | variable kg/m$^3$ |
| $p_o$ | Initial phreatomagma pressure | variable Pa |
| $p_a$ | Final phreatomagma pressure | 15 MPa |
| d | Particle loading ratio (mass particles/mass of fluid) | variable |
| $-\Delta E$ | Explosion energy | J |
| conversion factor: | 1 Mt TNT = | 4.184x10$^{15}$ Joule |

In our model, the phreatomagma ($T_o$=1000 ℃) resides transiently at some depth corresponding to $p=p_o$. We first consider how varying the phreatomagma volume ($V_o$) and mass fraction of fluid ($\phi_f$) affect explosive yield (Fig. 5). The dark gray thick vertical line in Figure 5 depicts the pressure ratio assuming a vent pressure of 15 MPa, which corresponds to a vent 150 meters below mean sea level. If the pressure at the vent varied during the eruption then the ratio $p_a/p_o$ changes. The thick light blue horizontal lines in Figure 5 corresponds to the tsunami-based (Purkis et al., 2023; Chernogor & Luo, 2025) and preliminary estimates of explosive yield made early on (Yuen et al., 2022), whereas the thick light gray lines or regions correspond to estimates of explosive yield constrained by the atmospheric blast waves (Adushkin et al., 2022; Diaz & Rigby, 2022; Kulichkov et al., 2022; Vergoz et al., 2022). This disparity is consistent with the excess eruptive energy being partitioned between the solid Earth, ocean, and atmosphere (Henley et al., 2024; Chernogor & Luo, 2025). The preferred model result will ideally overlap with the intersection of the vertical gray line ($p_{vent}/p_o$) and the maximum explosive yield produced by the eruption (thick gray horizontal region). Note that the vent location may have deepened syn-eruption, which would move the vertical gray line to lower values along the x-axis, as seen in Fig. 5 when $p_o$ increases from 30 MPa to 50 MPa. Assuming the energy deposited in the atmosphere due to blast waves was ~150-200 Mt, then eruptive volumes in the range ~4.5-6.5 km$^3$ with reservoir initial pressure of approximately 50 MPa for $H_2O$-rich phreatomagma ($\phi_f \geq 0.4$) are internally consistent. For less-$H_2O$-rich scenarios ($\phi_f \leq 0.2$), the lower range of explosive yields (~150 Mt) can be reproduced by a volume of magma roughly equivalent to the erupted volumes reported by Seabrook et al. (2023) when $p_o$ = 30 MPa. However, given that the eruption duration (~11 hours; Van Eaton et al., 2023) far exceeded the time period considered in our explosion model, it is unlikely that this maximum volume of magma was involved in the most intense explosion of the 15 January 2022 eruption, and we favor a model result with a lower volume. Because of uncertainties in measured energies and the trade-off between values in the explosion model, other conditions are possible although certain combinations can be ruled out. It is interesting to note (Fig. 5, panel A) that the estimated explosion energy of Krakatau

(100-150 Mt)--the eruption Hunga is most often compared to (e.g. Díaz & Rigby, 2022; Matoza et al., 2022; Yuen et al., 2022; Purkis et al., 2023)-- was in the same explosive energy range as Tonga, but the Krakatau erupted magma was two to three times more voluminous at roughly 10 to 20 $km^3$ for (Lipman, 2000; Mader, 2006). This feature itself highlights the extraordinary effects played by the interaction of pristine magma with copious amounts of seawater to produce the extreme behavior of the Hunga plume, notably its record maximum altitude of ~58 km (Mastin et al., 2024).

Figure 6 portrays the explosive yield versus the ratio of the vent to reservoir pressure at a reservoir temperature of 1100 ℃ for various fluid mass fractions and various reservoir (initial) pressures. The vertical color-coded bars assume a vent pressure of 15 MPa, corresponding to a vent at 150 m below sea level. The eruptive volume is fixed at 5 $km^3$ which is close to the volcanological observations of pyroclastic deposits on the sea floor (Clare at al., 2023; Kelly et al., 2024; Henley et al., 2024) and estimates in the 5-6.85 $km^3$ range. Given the target explosive yield for the atmospheric blast waves of 150-200 Mt, one may deduce reservoir pressures in the 50 to 70 MPa range for high mass fractions of fluid. Under lithostatic conditions, using a nominal crustal density of 2650 $kg/m^3$, this pressure range corresponds to a range of reservoir depths of ~2-3 km below sea level, within the range reported by Wu et al. (2025) of 2-5.5 km for the magmatic reservoir. The right panel shows the vent (exit) temperature following decompression as a function of the pressure ratio. For magma bodies of identical volume, $T_{exit}$ is insensitive to changes in $p_o$, and is instead governed by the mass fraction of fluid in the system, as depicted in the right panel. For example, initial reservoir pressures of 50-70 MPa with concomitant vent to initial pressure ratios ~ 0.03, vent exit temperatures are in the range 400-620 ℃ for fluid mass fractions of 0.5-0.8 in the phreatomagmatic plume, consistent with plume $H_2O$ contents postulated above based upon plume geometry and $H_2O$ loading . Although we are not aware of vent temperature measurements for Hunga, Shinohara (2005) reported vent temperatures in the range 390-680 ℃ for the $H_2O$-rich volcanic plumes at oceanic-arc volcanoes in Japan. These vent temperatures can place a lower constraint on reasonable exit temperatures of the phreatomagmatic mixture presented in Figure 6. Unrealistically low temperatures are computed at low vent/initial pressure ratios for plumes with fluid mass fractions greater than ~0.4, which rules out initial reservoir pressures greater than a few hundred MPa in the isentropic model.

Evidently, the spectacular height of the Hunga eruptive plume was due in significant measure to the profound interaction of magma, initially containing a typical amount of magmatic $H_2O$ (3-5 wt.%), with copious amounts of ingested sea water (Colombier et al., 2023, 2025; Mastin et al., 2024; Wu et al., 2025; Xu et al., 2022). Roughly 2 $km^3$ of pristine andesitic magma contains sufficient enthalpy to heat and flash the quantity of $H_2O$ contained in the plume explosion model. The mass of magma determined from calorimetry is, for the low $H_2O$ estimate $3.6 \times 10^{12}$ kg and for the high water estimate $10.1 \times 10^{12}$ kg values in overlapping agreement with the explosion models.

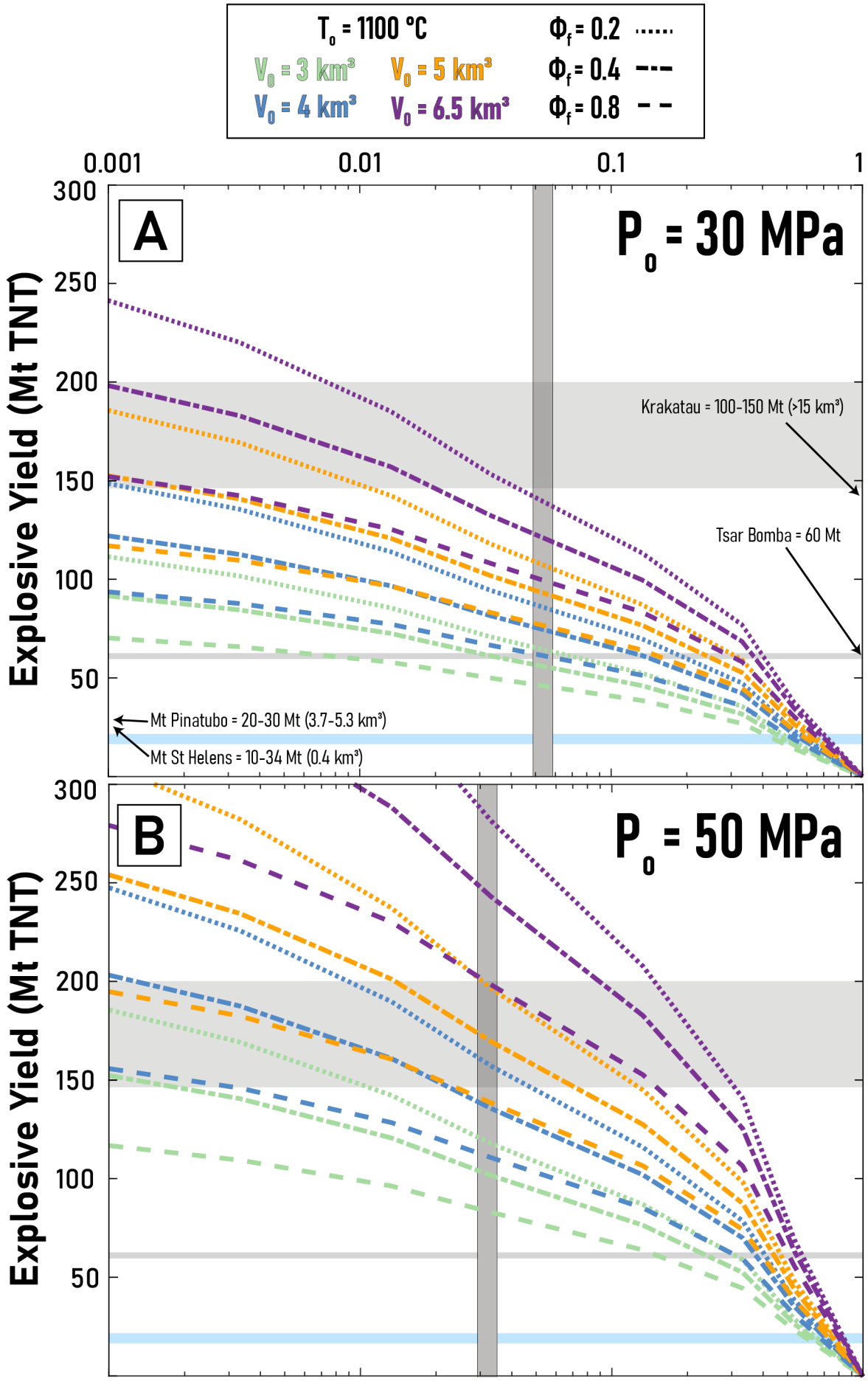
T0 = 1100 °C
V0 = 3 km³
V0 = 4 km³
V0 = 5 km³
V0 = 6.5 km³
Φf = 0.2
Φf = 0.4
Φf = 0.8
0.001
0.01
0.1
1
A
P0 = 30 MPa
B
P0 = 50 MPa
Explosive Yield (Mt TNT)
300
250
200
150
100
50
Krakatau = 100-150 Mt (>15 km³)
Tsar Bomba = 60 Mt
Mt Pinatubo = 20-30 Mt (3.7-5.3 km³)
Mt St Helens = 10-34 Mt (0.4 km³)

*Figure 5. Explosive yield as a function of pressure ratio for a magma reservoir located at a depth equivalent to P=30 MPa (panel A) and P=50 MPa (panel B). Different volumes of magma are shown as different colors. A thicker, horizontal blue line denotes a range of lower estimates 18-20 Mt TNT; from Yuen et al. (2022), the cumulative E of Purkis et al. (2023), and Chernogor & Luo (2025) for the climactic Hunga eruption. Upper estimates of explosive yield range from 61-200 Mt TNT (Adushkin et al., 2022; Diaz & Rigby, 2022; Kulichkov et al., 2022; Vergoz et al., 2022) and are illustrated by the grey horizontal lines in the plot background. Explosive yields from other volcanic eruptions and historical explosions are displayed for reference. The model assumes isentropic expansion (adiabatic and reversible) and is constrained by estimates of yield and measured water depth. A volume of magma of ~5 $km^3$ gives the best fit when $P_o$ = 50 MPa, as the estimated Mt TNT overlaps the range of observed Mt TNT at $P_{vent}/P_o$. Notice that a volume of juvenile magma just exceeding the eruptive volume is required to reproduce the observed Mt TNT when $P_o$ = 30 MPa.*

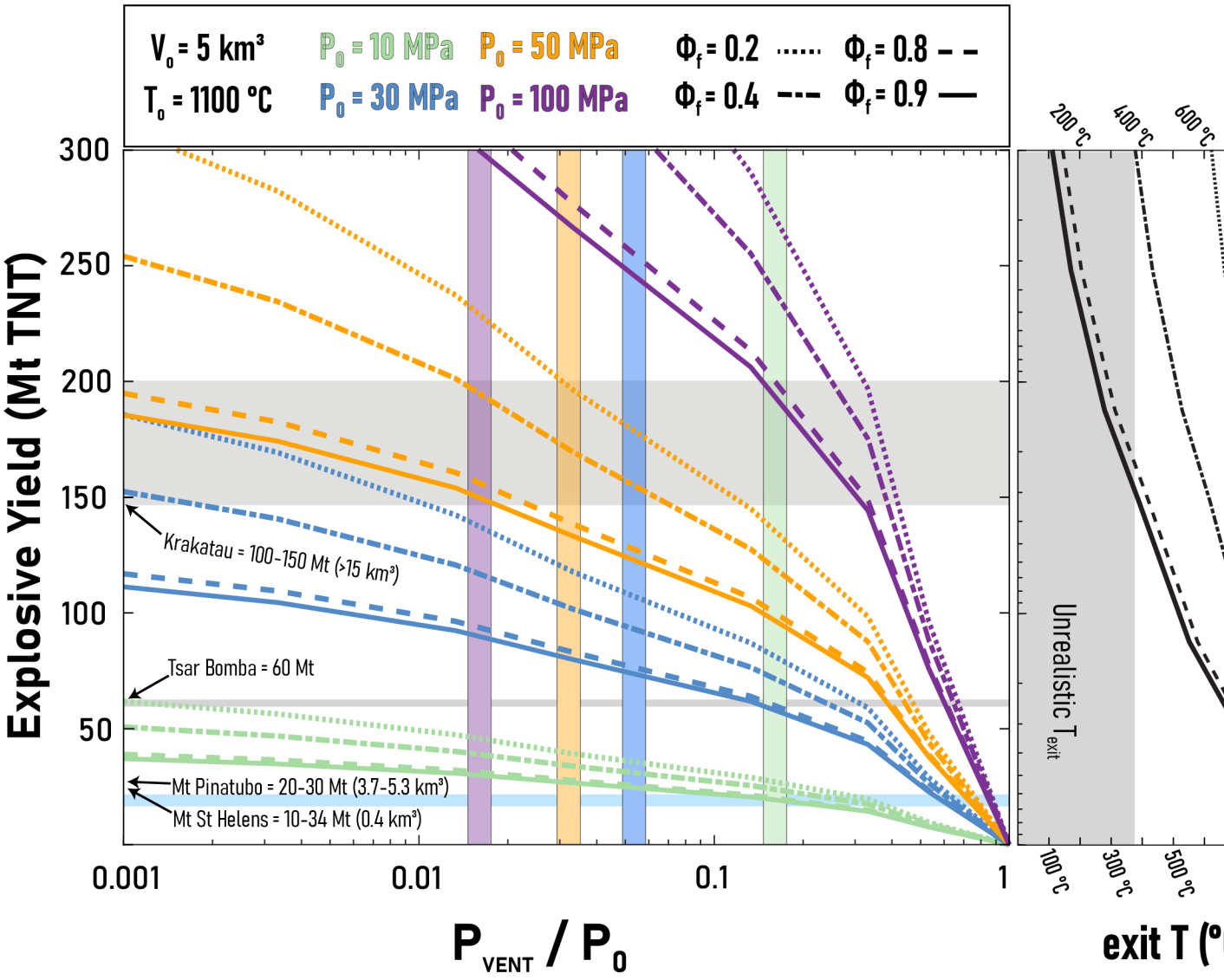


*Figure 6. Same as Figure 5 but for a $V_o$=5 km³ magma body, illustrating explosive yield as a function of pressure (left) and temperature (right). $P_{vent}/P_O$ for a vent located at ~150 m b.s.l. are illustrated by the vertical lines with colors corresponding to the model results. A thicker, horizontal blue line denotes a range of lower estimates 18-20 Mt TNT; from Yuen et al. (2022), the cumulative E of Purkis et al. (2023), and Chernogor & Luo (2025) for the climactic Hunga eruption. Upper estimates of explosive yield range from 61-200 Mt TNT (Adushkin et al., 2022; Diaz & Rigby, 2022; Kulichkov et al., 2022; Vergoz et al., 2022) and are illustrated by the grey horizontal lines in the plot background. Explosive yields from other volcanic eruptions and historical explosions are displayed for reference. The mass fractions of fluid isopleths in right panel are keyed to the figure legend at top of left panel.*

**Comparison of models**

Our modeling suggests that extensive interactions between magma and seawater led to the huge plume and high explosive yield. The interactions occurred at a minimal depth of 150 m below sea level and may have significantly deepened during the eruption. Limited tephra ascended into the atmosphere, whereas extensive deposits remained under water and were emplaced on the flanks (Clare et al. 2023; Colombier et al., 2025; Wu et al., 2025). Our model stands in contrast to that of Henley et al. (2024) who suggest that a large slug of gas in a cavity that was suddenly breached caused the main blast. Mastin et al. (2024) focused on modeling of the plume, using empirical relationships between plume height and eruption rate. They inferred the mass of water to be $2.88 \times 10^{12}$ kg (see Wu et al., 2025), a value extremely close to our estimates and based on completely independent methods.

There are critical limitations to the various models. Our model requires a series of blasts and a ratio of magma to seawater of about 1:1 to produce explosive activity (Wohletz, 1986). Our scenario then may need special conditions to achieve this 1:1 ratio (Wohletz 1986). For the time scale, we note that seismic data showed 4 main pulses over 300 sec (Zheng et al., 2023). This duration is consistent with the rise time (first ¼ cycle) of the Lamb wave (Matoza et al. 2022). The eruption was not a single "pop", but rather a series of explosive events. The recording of a series of sonic booms in Tonga's capital (Yuen et al., 2022) further supports this view, as does the strongly pulsative nature of the lightning activity in the eruption (Bór et al., 2023).

Henley et al's (2024) model requires a rather long time (we estimate this to be ~20-30,000 years) to concentrate gases and to allow the creation and maintenance of a strong seal. The fact that there was a significant eruption on January 14, the day before the cataclysmic event, suggests that a possible seal was already breached and likely had not completely resealed. The January 14 eruption may have occurred from a different vent, perhaps adjacent to the January 15 vent. It is thus possible that a breached, adjacent vent may have caused a depressurization of the primary magma chamber.

If the gas scenario proffered by Henley et al. (2024) is true, then why would the system "seal" or reseal itself four or more times (once for each of the four seismic events)? It seems more likely that it would only breach once, after which the pressure would be reduced. We envisage the four seismic events as representing strong pulses of activity as new batches of magma came into contact with seawater.

Four factors are consistent with a relatively small amount of magma reaching the surface (a.s.l.):

1) The small amount of airfall ash (0.1 to 0.2 $km^3$; Mastin et al., 2024);
2) The low observed $SO_2$ volume (0.6 Mt; Carn et al., 2022). One explanation for this is "scrubbing" of the $SO_2$ by seawater (Carn et al., 2022; Colombier et al., 2025; Wu et al., 2025).
3) The amount of water vapor in the stratosphere (up to 146 Tg; Millan et al., 2022, Zhu et al., 2022, Vomel et al., 2022)
4) The calorimetry needed to flash seawater to steam (this paper, section Eruption Thermal Calorimetry)

We believe our model is more plausible based on Occam's Razor (Walsh, 1979). It was a potentially typical – but large - eruption (simple) that happened to occur under several hundred

meters of water (adding complications). Henley et al's. (2024) model, in contrast, requires an unprecedented concentration of hot gas under a long-lasting strong and tight seal. We cannot rule out that some extra gas (steam) was involved. Mastin et al. (2024) also concluded that the eruption was gas-rich. The question then becomes, what is the source of the extra gas? We argue that the most likely source was seawater flashed to steam. We followed a different path than prior studies (Mastin et al., 2024; Colombier et al., 2025; Wu et al., 2025) but come to similar conclusions about the important role of seawater.

## Conclusions

Plume volumes were estimated using observed areas from satellite data and estimated thicknesses. Here we assume that the excess water is seawater, in contrast to Henley et al. (2024) who assumed a large gas phase sealed at depth prior to the eruption. Water concentrations were estimated from the thunderstorm literature and calculations for several Alaskan volcanoes.

Our results show that the Hunga plume contained 2.7-3.5 x $10^{12}$ kg water. In contrast, the water dissolved in the magma (assuming 6.85 $km^3$) was only 5.4-8.9 x $10^{11}$ kg water. This suggests that the visible plume was ~80 % seawater.

We calculated the volume of magma needed to heat the seawater and flash it into steam; this is 1.4-3.1 $km^3$ based on simple calorimetry. The likely volume change under the surface was 6.85 $km^3$, so the volume of magma needed to supply the necessary heat is available.

A simple isentropic explosion model and use of typical thermodynamic properties of magma and $H_2O$ and an assumed range of initial conditions provide estimates of the explosion energy consistent with the energy deposited by blasts into the atmosphere. A somewhat higher value of 4-5 $km^3$ of magma is needed to best support the yield estimates, depending on the proportions of water to magma in the phreatomagmatic mixture (Figure 5). Our results have implications for providing constraints on eruption mechanisms and estimating the explosive yield.

## Acknowledgements

We thank C. Vagasky and R. Said (Vaisala) for lightning data, K. Bedka (NASA) for plume height estimates, and P. Webley (UAF) for help with remote sensing data. Suggestions by O. Roche, M. Colombier and an anonymous reviewer helped to improve the manuscript. A.J. McNutt helped with Figure 4. FJS acknowledges continual support from the National Science Foundation (EAR) and US Department of Energy (geothermal and BES) for the past five decades. There was no external funding for this project specifically.

Appendix A – Augustine and Redoubt plume volume estimates
Appendix B – Cloud Water Contents for various thunderstorms
Appendix C – Hunga water estimates at different times

## References.

Adushkin, V.V., Rybnov, Y.S. and Spivak, A.A. (2022) Geophysical effects of the eruption of Hunga-Tonga-Hunga-Ha'apai Volcano on January 15, 2022. *Doklady Earth Sciences*, 504, 632-367. doi: 10.1134/s1028334X22060034

Baron, A., Chazette, P., Khaykin, S., Payen, G., Marquestaut, N., Bègue, N., and Duflot, V. (2023). Early evolution of the stratospheric aerosol plume following the 2022 Hunga Tonga-Hunga Ha'apai eruption: Lidar observations from reunion (21 S, 55 E). *Geophysical Research Letters*, *50*(10), e2022GL101751.

Bór, J., Bozóki, T., Sátori, G., Williams, E., Behnke, S. A., Rycroft, M. J., et al. (2023). Responses of the AC/DC global electric circuit to volcanic electrical activity in the Hunga Tonga-Hunga Ha'apai eruption on 15 January 2022. Journal of Geophysical Research: Atmospheres, 128, e2022JD038238. https://doi.org/10.1029/2022JD038238

Brenna, M., Cronin, S. J., Smith, I. E., Pontesilli, A., Tost, M., Barker, S., ... and Vaiomounga, R. (2022). Post-caldera volcanism reveals shallow priming of an intra-ocean arc andesitic caldera: Hunga volcano, Tonga, SW Pacific. *Lithos*, *412*, 106614.

Buresti, G., and Casarosa, C. (1989). One-dimensional adiabatic flow of equilibrium gas–particle mixtures in long vertical ducts with friction. *Journal of Fluid Mechanics*, *203*, 251-272.

Cahalan, R. C., and Dufek, J. (2021). Explosive submarine eruptions: The role of condensable gas jets in underwater eruptions. *Journal of Geophysical Research: Solid Earth*, *126*(2), e2020JB020969.

Carn, S. A., Krotkov, N. A., Fisher, B. L., and Li, C. (2022). Out of the blue: Volcanic SO2 emissions during the 2021–2022 eruptions of Hunga Tonga—Hunga Ha'apai (Tonga). *Frontiers in Earth Science*, *10*, 976962.

Carr, J. L., Horváth, Á., Wu, D. L., and Friberg, M. D. (2022). Stereo plume height and motion retrievals for the record-setting Hunga Tonga-Hunga Ha'apai eruption of 15 January 2022. *Geophysical Research Letters*, *49*(9), e2022GL098131. doi: 10.1029/2022GL098131

Chernogor, L. and Luo, Y. (2025) Statistical analysis of seismic and tsunami waves generated by the 2022 Tonga Volcano's eruption. *In:* Nemeth, K. (ed.), *A comprehensive study of volcanic phenomena*. IntechOpen, London, p. 163-185. doi: 10.5772/intechopen.1006881

Cimarelli, C., Behnke, S., Genareau, K., Méndez Harper, J. and van Eaton, A.R. (2022) Volcanic electrification: recent advances and future perspectives. *Bulletin of Volcanology*, 84, 78. doi: 10.1007/s00445-022-01591-3

Clare, M. A., Yeo, I. A., Watson, S., Wysoczanski, R., Seabrook, S., Mackay, K., ... and Williams, M. (2023). Fast and destructive density currents created by ocean-entering volcanic eruptions. *Science*, *381*(6662), 1085-1092.

Colombier, M., Ukstins, I. A., Tegtmeier, S., Scheu, B., Cronin, S. J., Thivet, S., ... and Dingwell, D. B. (2023). Atmosphere injection of sea salts during large explosive submarine volcanic eruptions. *Scientific Reports*, *13*(1), 14435.

Colombier, M., Bonifacie, M., Brenna, M., Burke, A., Cimarelli, C., Cronin, S. J., ... and Wu, J. (2025). The role of submarine volcanism in atmospheric chemistry. *Earth and Planetary Science Letters*, *671*, 119690.

Coombs, M. L., Bull, K. F., Vallance, J. W., Schneider, D. J., Thoms, E. E., Wessels, R. L., and McGimsey, R. G. (2010). Timing, distribution, and volume of proximal products of the 2006 eruption of Augustine Volcano. *The 2006 eruption of Augustine volcano, Alaska, USGS Prof. Paper 1769*, 145-186.

Díaz, J. S., and Rigby, S. E. (2022). Energetic output of the 2022 Hunga Tonga–Hunga Ha ‘apai volcanic eruption from pressure measurements. *Shock Waves*, *32*(6), 553-561.

Dogan, G. G., Yalciner, A. C., Annunziato, A., Yalciner, B., and Necmioglu, O. (2023). Global propagation of air pressure waves and consequent ocean waves due to the January 2022 Hunga Tonga-Hunga Ha'apai eruption. *Ocean Engineering*, *267*, 113174.

Donner, S., Steinberg, A., Lehr, J., Pilger, C., Hupe, P., Gaebler, P., Ross, J.O., Eibl, E.P.S., Heimann, S., Rebscher, D., Plenefisch, T. and Ceranna, L. (2023) The January 2022 Hunga Volcano explosive eruption from the multitechnological perspective of CTBT monitoring. *Geophysical Journal International*, 235, 48-73. doi: 10.1093/gji/ggad204

Dye, J. E., and Coauthors (1986), Early electrification and precipitation development in a small isolated Montana cumulonimbus. *J. Geophys. Res*., 91 (D1), 1231–1247.

Dye, J.E., J. J. Jones, A. J. Weinheimer and W. P. Winn (1988), Observations within two regions of charge during initial thunderstorm electrification, *Quart. J. Roy. Met. Soc*., 114, 1271-1290.

Folland, C. K., Salinger, M. J., and Rayner, N. (1997). A comparison of annual South Pacific island and ocean surface temperatures. *Weather and Climate*, 23-41.

Geotis, S. G. (1971). Thunderstorm water contents and rain fluxes deduced from radar. *Journal of Applied Meteorology (1962-1982)*, 1233-1237.

Gupta, A. K., Bennartz, R., Fauria, K. E., and Mittal, T. (2022). Eruption chronology of the December 2021 to January 2022 Hunga Tonga-Hunga Ha’apai eruption sequence. *Communications Earth & Environment*, *3*(1), 314.

Haar, L. (1984). *NBS/NRC steam tables*. CRC Press.

Henley, R.W., de Ronde, C.E.J., Arculus, R.J., Hughes, G., Pham, T., Casas, A.S., Titov, V. and Walker, S.L. (2024) The 15 January 2022 Hunga (Tonga) eruption: a gas-driven climactic

explosion. *J. Volcanology & Geothermal Res.*, 451, 108077. doi: 10.1016/j.volgeores.2024.108077

Heymsfield, A.J., A. Bansemer, G. Heymsfield, and A. O. Fierro (2009), Microphysics of maritime tropical convective updrafts at temperatures from -20C to -60C, *J. Atmos. Sci*., 66, 3530-3562.

Horvath, A., Vadas, S. L., Stephan, C. C., and Buehler, S. A. (2024). One-minute resolution GOES-R observations of Lamb and gravity waves triggered by the Hunga Tonga-Hunga Ha'apai eruptions on 15 January 2022. *Journal of Geophysical Research: Atmospheres*, *129*(3), e2023JD039329. GOES R

Kelly, L. J., Fauria, K. E., Manga, M., Cronin, S. J., Latu'ila, F. H., Paredes-Mariño, J., ... and Bennartz, R. (2024). Airfall volume of the 15 January 2022 eruption of Hunga volcano estimated from ocean color changes. *Bulletin of Volcanology*, *86*(6), 59.

Kintner, J. A., Yeck, W. L., Earle, P. S., Prejean, S., & Pesicek, J. D. (2023). High-precision characterization of seismicity from the 2022 Hunga Tonga-Hunga Ha'apai volcanic eruption. *Bull. Seismological Society of America*, *94*(2A), 589-602.

Kulichkov, S.N., Chunchuzov, I.P., Popov, O.E., Gorchakov, G.I., Mishenin, A.A., Perepelkin, V.G., … and Tikhonov, A.V. (2022) Acoustic-gravity Lamb waves from the eruption of the Hunga Tonga-Hunga Ha'apai Volcao, its energy release and impact on aerosol concentrations and tsunami. *Pure and Applied Geophysics*, 179, 1533-1548. doi: 10.1007/s00024-022-03046-4

Le Mével, H.E., Miller, C.A., Ribo, M., Cronin, S. and Kula, T. (2023) The magmatic system under Hunga volcano before and after the 15 January 2022 eruption. *Science Advances*, 9(50), eadh3156. doi: 10.1126/sciadv.adh3156

Lipman, P., 2000. Calderas. In: Sigurdsson, H., Houghton, B., Rymer, H., Stix, J., McNutt, S.(Eds.), The Encyclopedia of Volcanoes, pp. 113–141.

Lesher, C.E., and Spera, F.J., 2015. Thermodynamic and Transport Properties of Silicate Melts and Magma. In: Sigurdsson, H., Houghton, B., Rymer, H., Stix, J., McNutt, S. (Eds.), 2nd edition, The Encyclopedia of Volcanoes, pp. 643–662.

Mader, Charles. (2006). Numerical Modeling for the Krakatoa Hydrovolcanic Explosion and Tsunami. *Science of Tsunami Hazards*. 24. 174.

Maeno, F., Kaneko, T., Ichihara, M., Suzuki, Y. J., Yasuda, A., Nishida, K., and Ohminato, T. (2022). Seawater-magma interactions sustained the high column during the 2021 phreatomagmatic eruption of Fukutoku-Oka-no-Ba. *Communications Earth & Environment*, *3*(1), 260. doi: 10.1038/s43247-022-00594-4

Mastin, L. G., Van Eaton, A. R., and Cronin, S. J. (2024). Did steam boost the height and growth rate of the giant Hunga eruption plume?. *Bulletin of Volcanology*, *86*(7), 64.

Matoza, R. S., Fee, D., Assink, J. D., Iezzi, A. M., Green, D. N., Kim, K., ... and Wilson, D. C. (2022). Atmospheric waves and global seismoacoustic observations of the January 2022 Hunga eruption, Tonga. *Science*, *377*(6601), 95-100. doi: 10.1126/science.abo7063

Millan, L., Santee, M. L., Lambert, A., Livesey, N. J., Werner, F., Schwartz, M. J., ... and Froidevaux, L. (2022). The Hunga Tonga-Hunga Ha'apai hydration of the stratosphere. *Geophysical Research Letters*, *49*(13), e2022GL099381.

Pavolonis, M. J., Sieglaff, J. M., and Cintineo, J. L. (2020). Remote sensing of volcanic ash with the GOES-R series. In *The GOES-R Series* (pp. 103-124). Elsevier.

Petersen, W. A., and Rutledge, S. A. (1998). On the relationship between cloud-to-ground lightning and convective rainfall. *J. Geophysical Research: Atmospheres*, *103*(D12), 14025-14040.

Plank, T., Kelley, K. A., Zimmer, M. M., Hauri, E. H. and Wallace, P. J. (2013).Why do mafic arc magmas contain ~4 wt% water on average? *Earth Planet. Sci. Lett*. 364, 168–179.

Poli, P., & Shapiro, N. M. (2022). Rapid characterization of large volcanic eruptions: Measuring the impulse of the Hunga Tonga Ha'apai explosion from teleseismic waves. *Geophysical Research Letters*, *49*(8), e2022GL098123.

Purkis, S. J., Ward, S. N., Fitzpatrick, N. M., Garvin, J. B., Slayback, D., Cronin, S. J., ... and Dempsey, A. (2023). The 2022 Hunga-Tonga megatsunami: Near-field simulation of a once-in-a-century event. *Science advances*, *9*(15), eadf5493.

Rakov, V.A. and M.A. Uman, (2003). Lightning—Physics and Effects, Cambridge University Press.

Rudinger, G. (1976). Fundamentals and applications of gas-particle flow. *In AGARD Flow of Solid Particles in Gases p 55-86 (SEE N77-12352 03-34*, 55-86.

Schmid, F., Petersen, G., Hooft, E., Paulatto, M., Chrapkiewicz, K., Hensch, M., and Dahm, T. (2022). Heralds of future volcanism: Swarms of microseismicity beneath the submarine Kolumbo volcano indicate opening of near-vertical fractures exploited by ascending melts. *Geochemistry, Geophysics, Geosystems*, *23*(7), e2022GC010420.

Seabrook, S., Mackay, K., Watson, S. J., Clare, M. A., Hunt, J. E., Yeo, I. A., ... and Williams, M. J. (2023). Volcaniclastic density currents explain widespread and diverse seafloor impacts of the 2022 Hunga Volcano eruption. *Nature communications*, *14*(1), 7881.

Shakespeare, C. J., and Roderick, M. L. (2024). What Controls Near-Surface Relative Humidity Over the Ocean?. *Journal of Advances in Modeling Earth Systems*, *16*(6), e2023MS004168.

Shinohara, H. (2005). A new technique to estimate volcanic gas composition: plume measurements with a portable multi-sensor system. *J. Volcanology and Geothermal Research*, 143, 319-333.

Sisson, T. W., & Grove, T. L. (1993). Experimental investigations of the role of H2O in calc-alkaline differentiation and subduction zone magmatism. *Contributions to mineralogy and petrology*, *113*(2), 143-166.

Smart, D. (2022). The first hour of the paroxysmal phase of the 2022 Hunga Tonga–Hunga Ha'apai volcanic eruption as seen by a geostationary meteorological satellite. *Weather*, *77*(3), 81-82.

Stith, J.L., J. Haggerty, C. Grainger, and A. Detwiler (2006), A comparison of the microphysical and kinematic characteristics of mid-latitude and tropical convective updrafts and downdrafts, *Atmos. Res*., 82, 350-366.

Thompson, G., S.R. McNutt, M. Scruggs, F. Spera, Y. Zheng, Z. Peng, K. Mandli, D. Yuen, and C. Vagasky (2022). Hunga-Tonga Games: Unravelling the Timing and Size of the Biggest Volcanic Explosion in 30 Years. Abstract, SSA Meeting, Bellevue, WA, April 2022.

Van Eaton, A. R., Lapierre, J., Behnke, S. A., Vagasky, C., Schultz, C. J., Pavolonis, M., ... and Khlopenkov, K. (2023). Lightning rings and gravity waves: Insights into the giant eruption plume from Tonga's Hunga Volcano on 15 January 2022. *Geophysical Research Letters*, *50*(12), e2022GL102341.

Vergoz, J., Hupe, P., Listowski, C., Le Pichon, A., Garcés, M.A., Marchetti, E., Labazuy, P., Ceranna, L., Pilger, C., Gaebler, P., Näsholm, S.P., Brissaud, Q., Poli, P., Shapiro, N., De Negri, R. and Mialle, P. (2022) IMS observations of infrasound and acoustic-gravity waves produced by the January 2022 volcanic eruption of Hunga, Tonga: a global analysis. *Earth and Planetary Science Letters*, 591, 117639. doi: 10.1016/j.epsl.2022.117639

Vömel, H., Evan, S., and Tully, M. (2022). Water vapor injection into the stratosphere by Hunga Tonga-Hunga Ha'apai. *Science*, *377*(6613), 1444-1447.

Wallis, G.B. (1969) One Dimensional Two-Phase-Flow, 1408, McGraw-Hill, New York.

Walsh, D. (1979) Occam's Razor: a principle of intellectual elegance. *American Philosophical Quarterly*, 16(3), 241-244. https://www.jstor.org/stable/20009764

Weinheimer, A.J., J. E. Dye, D. W. Breed, M.P. Spowart, J. L. Parrish, T. L. Hoglin and T.C. Marshall (1991), Simultaneous measurements of the charge, size, and shape of hydrometeors in an electrified cloud, *J. Geophys. Res*., 96,20,809-20,829.

Williams, E. R., and McNutt, S. R. (2005). Total water contents in volcanic eruption clouds and implications for electrification and lightning. *Recent progress in lightning physics*, *81*, 93.

Wohletz, K.H. (1986) Explosive magma-water interactions: thermodynamics, explosion mechanisms, and field studies. *Bulletin of Volcanology*, 48, 245-64. doi: 10.1007/BF01081754

Wu, J., Cronin, S. J., Brenna, M., Park, S. H., Pontesilli, A., Ukstins, I. A., ... & Kula, T. (2025). Low sulfur emissions from 2022 Hunga eruption due to seawater–magma interactions. *Nature Geoscience*, 1-7.

Xu, J., Li, D., Bai, Z., Tao, M., & Bian, J. (2022). Large amounts of water vapor were injected into the stratosphere by the Hunga Tonga–Hunga Ha'apai volcano eruption. *Atmosphere*, *13*(6), 912.

Yuen, D. A., Scruggs, M. A., Spera, F. J., Zheng, Y., Hu, H., McNutt, S. R., ... & Tanioka, Y. (2022). Under the surface: Pressure-induced planetary-scale waves, volcanic lightning, and gaseous clouds caused by the submarine eruption of Hunga Tonga-Hunga Ha'apai volcano. *Earthquake Research Advances*, *2*(3), 100134.

Zheng, Y., Hu, H., Spera, F. J., Scruggs, M., Thompson, G., Jin, Y., ... & Yuen, D. A. (2023). Episodic magma hammers for the 15 January 2022 cataclysmic eruption of Hunga Tonga-Hunga Ha'apai. *Geophysical Research Letters*, *50*(8), e2023GL102763.

Zhu, Y., Bardeen, C. G., Tilmes, S., Mills, M. J., Wang, X., Harvey, V. L., ... & Toon, O. B. (2022). Perturbations in stratospheric aerosol evolution due to the water-rich plume of the 2022 Hunga-Tonga eruption. *Communications Earth & Environment*, *3*(1), 248.

Zhu, Y., Portmann, R. W., Kinnison, D., Toon, O. B., Millán, L., Zhang, J., ... & Rosenlof, K. H. (2023). Stratospheric ozone depletion inside the volcanic plume shortly after the 2022 Hunga Tonga eruption. *Atmospheric Chemistry and Physics*, *23*(20), 13355-13367.

Zimanowski, B., Büttner, R., Dellino, P., White, J.D.L., & Wohletz, K.H., 2015. Magma-Water interaction and phreatomagmatic fragmentation. In: Sigurdsson, H., Houghton, B., Rymer, H., Stix, J., McNutt, S. (Eds.), 2nd edition, The Encyclopedia of Volcanoes, pp. 473-484.